Minerals Engineering 231 (2025) 109480

Contents lists available at ScienceDirect

Minerals Engineering

journal homepage: www.elsevier.com/locate/mineng

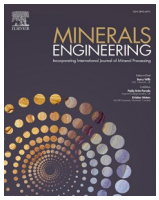

Exploring phosphorus dissociation kinetics in HCl-leached moderate-grade phosphate ores: Towards high-quality dicalcium phosphate production

Hassan H.A. Younes [a,b], Lei Qin [a], Abdelaal S.A. Ahmed [c], Feifei Jia [a], Shaoxian Song [a], Weiquan Zhan [d,*]

[a] School of Resources and Environmental Engineering, Wuhan University of Technology, Wenzhi Street 34, Wuhan, Hubei 430070, China
[b] Mining and Petroleum Engineering Department, Faculty of Engineering, Al-Azhar University, Qena 83513, Egypt
[c] Chemistry Department, Faculty of Science, Al-Azhar University, Assiut 71524, Egypt
[d] Instituto de Física, Universidad Autonoma de San Luis Potosí, Av. Manuel Nava 6, Zona Universitaria, San Luis Potosí 78290, Mexico

ARTICLE INFO

Keywords:
Phosphate ore
HCl leaching
Dissociation kinetics
P_2O_5 recovery
Particle size

ABSTRACT

Reaction kinetics is crucial for understanding process mechanisms and plays a key role in the recovery of phosphorus extraction, providing essential insights for optimization and scaling up, which directly impact profitability and engineering design. This article focuses on the comprehensive study of the reaction kinetics involved in phosphorus extraction from apatite mineral using prepared HCl, emphasizing its significance for efficient resource utilization and process enhancement. The impacts of acid concentration, solid-to-liquid ratio, particle size fractions, agitation rate, and temperature on the dissolution rate were meticulously evaluated. The dissolution kinetics of phosphorus extraction from apatite using heterogeneous reaction models, identifying the best-fitting equation for experimental data. A P_2O_5 extraction rate of 99.93 % was achieved at 14 °C with (+0.063–0.15) mm particles after 90 s. The variance coefficient (*CV*) of the typical sample was calculated to be 112 %. Shrinking Core Models (SCMs) were employed to determine the rate-controlling phase of the leaching process, leading to a semi-empirical kinetic equation for P_2O_5 leaching. The activation energy was found to be 15.88 kJ/mol using the Arrhenius equation. Energy dispersive X-ray spectroscopy (EDS), X-ray diffraction (XRD), and Fourier transform infrared spectroscopy (FT-IR) analyses confirmed silica residue. This work sheds light on phosphorus extraction kinetics, aiming at optimizing the process conditions, designing efficient reactors, and assessing the operation's economic viability.

1. Introduction

Phosphorite, is a type of rock that contains a significant quantity of apatite, with the general formula $(Ca_{10}(PO_4)_6$ (anion group)$_2$, where "anion group" can be F^-, Cl^-, and OH^-(Martin B. Hocking, 2005). It can be either volcanic or sedimentary in nature and serve as the primary ingredient in the manufacturing of phosphoric acid (Becker Pierre, 1983). Additionally, it is an essential mineral resource that has extensive uses in multiple industries, particularly in the manufacturing of fertilizers, chemicals, and food products (Hao et al., 2014; Orabi et al., 2018). Phosphorus is vital for sustaining the optimal functioning of human beings as it plays a role in numerous fundamental biological processes (Ferket et al., 2002). Feed phosphates are chemically synthetic substances used as a supplement in animal feed for a variety of animals, such as pets, chickens, cattle, and fish (European Commission, 2010). Defluorinated calcium phosphate (DFP) is a crucial component of these feed phosphates, which also include monocalcium phosphate (MCP) and dicalcium phosphate (DCP) (Sullivan et al., 1994).

Depending on their principal gangue constituents, phosphorite ores vary greatly. By main impurities, phosphate rocks are classified as siliceous ores, clayey ores, sedimentary calcium-based ores, organic phosphate ores, and complicated mineralogical phosphate ores (Abouzeid, 2008; Khoshjavan and Rezai, 2011). Two essential procedures are used to extract phosphoric acid from phosphorite for industrial manufacturing (Gilmour, 2013). The first method, referred to as the "dry process", yields furnace acid. This procedure entails combusting yellow phosphorus in the existence of air as an intermediary phase, followed by the reaction of the resultant phosphorus pentoxide with water. Another approach involves acidifying phosphate rock with mineral or organic acids, often known as "wet processes". Recognizing the significant

* Corresponding author.
E-mail address: zhan_weiquan@163.com (W. Zhan).

https://doi.org/10.1016/j.mineng.2025.109480
Received 5 January 2025; Received in revised form 29 April 2025; Accepted 29 May 2025
Available online 3 June 2025

energy consumption and pollutants associated with the thermal process, the wet process has been identified as the primary technique for phosphoric acid manufacturing offering advantages such as cost efficiency, widespread adoption for large-scale production, the ability to process lower-grade phosphate rocks, and prevention of P_2O_5 emissions (Lv et al., 2021; Ma et al., 2018).

An extensive analysis has been carried out on the kinetics of phosphate ore dissolving using various mineral acids(Bandara and Senanayake, 2019), including sulfuric (Sinirkaya et al., 2012), nitric (Olanipekun, 2003; Poissonnier et al., 2021), phosphoric (Elmisaoui et al., 2024), and hydrochloric (Azeez et al., 2024) acids, as well as Cl_2 (Abali et al., 1997) and SO_2 (Yartaşi et al., 1994) gases in a water-based solution. These acids were used individually or in combinations (Antar and Jemal, 2008; Ethiopia, 1999), and organic acids such as acetic (Arroug et al., 2021), oxalic (Mendes et al., 2020), and succinic (Ashraf et al., 2005) acids were also employed to extract valuable compounds from rock. Table 1 provides an overview of several reported kinetic expressions.

The sulfuric acid method is currently the most widely used technique in the phosphoric acid industry and is particularly favored for high-grade phosphate rock acidolysis due to its economic feasibility and relative simplicity (Lassis et al., 2015; Liu et al., 2021). However, its widespread use results in the generation of large amounts of phosphogypsum, a difficult-to-manage by-product. Currently, most phosphogypsum is discarded in vast stockpiles without treatment, with an annual increase of 200–280 million tons (Lv and Xiang, 2022). Excessive phosphogypsum requires substantial area for storage and contributes to environmental contamination as well (Rentería-Villalobos et al., 2010). Simultaneously, phosphate particles are readily covered by the phosphogypsum produced during sulfuric acid leaching, resulting in a reduced phosphate leaching yield (Wu et al., 2023). A promising alternative to the latter is the phosphogypsum-free technique, which employs hydrochloric acid.

The hydrochloric acid leaching method for phosphate ores is especially advantageous for processing complex, low-grade ores and producing high-purity phosphoric acid. HCl is a potent acid and a very tiny molecule. This is anticipated to have a more rapid diffusion rate compared to some other acids in the leaching process. Its ability to recover valuable by-products and avoid problematic gypsum waste provides both technical and economic benefits (Yu and Du, 2023). Due to the chemical characteristics of sulfuric and hydrochloric acids, which are monoprotic and diprotic acids respectively, hydrochloric acid leaching may need larger acid consumption than sulfuric acid techniques. Nonetheless, the financial gains from valuable by-products and the reduction of environmental obligations may counterbalance these costs. Moreover, Trade sulfuric acid is normally three to four times the price of by-product hydrochloric acid. This makes HCl leaching a strategic choice in high-value phosphate processing and resource recovery industries. Water-soluble calcium chloride and phosphoric acid are produced by dissolving phosphate ore with HCl (Soltani et al., 2017). Afterward, the phosphoric acid in the solution is removed using solvent extraction techniques to yield pure phosphoric acid (Abdel-Aal, 2000; Jin et al., 2014). For “high added value” applications like detergents and food additives, dry-produced phosphoric acid has less contaminants. Phosphoric acid from wet procedures is generally used to make fertilizers (Martin B. Hocking, 2005). The decision regarding which of such procedures is contingent upon variables such as the grade of the ore, the expenditure of energy, and the desired final outcome (Liu et al., 2022).

Kinetics is a field that is closely linked to profitability and engineering design. It has a broad variety of practical applications, including determining the quantity and amount of materials involved in a reaction, creating reactors, managing and optimizing processes, and scaling them up. The kinetic investigation of phosphoric ore dissolution holds fundamental significance, as it provides insights into the intricate mechanisms underlying the process. Gaining an exhaustive knowledge of such steps is vital for improving process conditions, developing efficient reactors, and evaluating the economic feasibility of the operation (Mgaidi and Mokni, 2018). It is further noted that the kinetics of the solid-lixiviant interactions during the leaching process are largely controlled by the shrinking core models (SCMs), which are heterogeneous in nature (Habbache et al., 2009; Liddell, 2005). Due to the absence of a product layer on the particles surfaces of unreacted phosphate ore, the leaching reaction with hydrochloric acid is consistently rapid (it has been recorded that the leaching efficiency of P_2O_5 exceeded 80 % within 6 min at a temperature of 45 °C) (Brahim et al., 2017). However, research on the kinetics of hydrochloric acid is somewhat scarce, particularly with low to medium-grade ores.

This study aimed to investigate the impact of acid concentration, solid-to-liquid ratio, particle size fraction, agitation speed, and reaction temperature on the rate at which phosphate rock dissociates in hydrochloric acid solutions. A mathematical model was applied to accurately describe the dissolving kinetics of phosphate ore, considering the influence of various parameters.

2. Experimental

Prior to delving into the detailed leaching experimental procedure, it is essential to underscore the reactions between phosphorite and hy-

Table 1
A review of some documented kinetic equations for phosphate ore digestion using different acids and their respective activation energies.*

Leaching agent (s)	Kinetic formulas	Ea [kJ/ mol]	Temp. Range	Ref.
H_2SO_4	$1–2/3x\text{-}(1\text{-}x)^{2/3} = kt$	17.6	60–90 °C	(Ethiopia, 1999)
H_2SO_4	$-\ln(1\text{-}x) = [k_o C_{acid}{}^{1.93} d_0^{-0.52} (S/L)^{-0.27} \exp^{-3567.52/T}]t^{0.7}$	29.66	14–70 °C	(Sevim et al., 2003)
H_2SO_4/HCl	$1–2/3x\text{-}(1\text{-}x)^{2/3} = kt$	13.3	60–90 °C	(Ethiopia, 1999)
HNO_3	$1\text{-}(2/3)x\text{-}(1\text{-}x)^{2/3} = kt$	14.2	40–70 °C	(Olanipekun, 2003)
HNO_3	$[H^+]/r_p = 1/k + SR/\alpha$	99.5	3–18 °C	(Bayramoglu et al., 1995)
HCl	$1–3(1\text{-}x)^{2/3} + 2(1\text{-}x) = 0.32 C_{acid}^{0.145} (S/L)^{-0.628} \exp^{(2600/T)} t$	21.6	25–45 °C	(Brahim et al., 2017)
HCl	$1–3(1\text{-}x)^{2/3} + 2(1\text{-}x) = k_o C_{acid}{}^{0.99} (L/S)^{-0.25} r_0{}^{-2.16} t$	1.5	20–50 °C	(Aly et al., 2013)
HCl	$1\text{-}(2/3)x\text{-}(1\text{-}x)^{2/3} = 0.65 C_{acid}^{0.789} d_0{}^{0.85} e^{(-4321RT)} t$	42.3	50–80 °C	(Ayinla et al., 2018)
HCl	$1\text{-}(1\text{-}x)^{1/3} = 7.6 * 10^{-6} C_{acid} (r_0)^{-1} \exp^{(-41990/RT)} t$	41.99	10–40 °C	(Lv et al., 2021)
HCl	$1\text{-}[1–0.7183x]^{1/3} = 3.8 * 10^{-7} C_{acid} (r_0)^{-1} \exp^{(-46000/RT)} t$ $x \leq 0.71$	46	10–40 °C	(Lv et al., 2021)
HCl	$1\text{-}[(1\text{-}x)/0.57]^{1/3} = 3.8 * 10^{-7} C_{acid} (r_0)^{-1} \exp^{(-46000/RT)} t$ x > 0.71	46	10–40 °C	(Lv et al., 2021)
H_2SO_4/ H_3PO_4	$-\ln(1\text{-}x) = 2.2*10^{-9} C_{acid}^{0.46} (S/L)^{0.75} G^{0.45} SR^{0.47} e^{(-2671/T)} t$	−18.48	25–40 °C	(Soussi-Baatout et al., 2016)
H_2SO_4/ H_3PO_4	$-\ln(1\text{-}x) = 2.2*10^{-9} C_{acid}^{0.46} (S/L)^{0.75} G^{0.45} SR^{0.47} e^{(-6959/T)} t$	−57.89	45–60 °C	(Soussi-Baatout et al., 2016)
H_3PO_4	$1–3(1\text{-}x)^{2/3} + 2(1\text{-}x) = 0.053 C_{acid}^{1.75} (L/S)^{-0.25} d_0{}^{-0.29} SR^{0.30} \exp^{(-3053/T)} t$	25.4 ± 1.8	25–65 °C	(Soussi-Baatout et al., 2018)

* Symbols used in Table1: x=P_2O_5 conversion linked to time; k = rate constant; k_o = rate coefficient; t = clock time; C_{acid} = acid concentration; r_0 = initial particle radius; d_0 = initial particle diameter; r_p = formation rate of H_3PO_4; SR = rotational stirring rate; α = coefficient of mass transfer; G = grain size fraction; L/S = liquid-to-solid ratio; S/L = solid-to-liquid ratio.

drochloric acid in precisely balanced quantities (Eqs.1–4).

$$Ca_{10}(PO_4)_6F_2 = 3Ca_3(PO_4)_2 + CaF_2 \quad (1)$$

$$Ca_3(PO_4)_2 = P_2O_5 + 3CaO \quad (2)$$

$$Ca_3(PO_4)_2 + 6HCl = 3CaCl_2 + 2H_3PO_4 \quad (3)$$

$$Ca_{10}(PO_4)_2F_2 + 20HCl = 6H_3PO_4 + 10CaCl_2 + 2HF \quad (4)$$

2.1. Material handling and preparation

The phosphate ore incorporated into this research weighed about 100 kg and was primarily composed of the output from the crushing circuit product (jaw crusher), exhibiting a size smaller than 4 mm. The sample was a kind of medium-grade banded phosphate rock (apatite). The provided ore originated from El-Naser Phosphate Company situated in Elsebaiya, Egypt. Following a comprehensive blending of the head sample, it was then divided into small samples using coning and quartering method. The thoroughly mixed samples were subsequently sealed tightly in plastic bags to maintain uniformity and keep them away from weathering circumstances to serve as a stock. The raw phosphate ore was then sieved to different size fractions. Through using ASTM standard sieves, equipped with an electric vibrating platform, the material underwent screening subsequent to being dried at 110 °C for a duration of 12 h. All the reagents used in this study (HCl, HNO_3, NH_4MoO_4, $NH_4V_2O_4$, and KH_2PO_4) provided by Shanghai Aladdin Biochemical Technology Co., Ltd. are of analytical grade. The used solvent was ultrapure water with resistivity of 18 MΩ.

2.2. Analysis and characterization

Approximately 50 g of the representative head sample were dried and ground well for both X-ray examinations. The chemical compositions of the ore head samples resulting from the crushing circuit were examined through X-ray fluorescence spectrum analysis. Using the ARL PERFORM'X X-ray fluorescence (XRF) sequential spectrometer. XRD investigations were conducted utilizing a DX-2007 X-ray diffraction spectrometer (Danton, China) employing a Cu Kα radiation source filtered via a graphite monochromator at a wavelength of λ = 1.54 nm. The voltage and anode current were 40 kV and 30 mA, respectively. Moreover, the morphological examination was executed with a Carl Zeiss ULTRA 55 Plus equipment (Germany) model scanning electron microscope equipped with EDX on an Oxford X Max 80 electron microscope (UK) and XRF on a Shimadzu EDX7000P spectrometer (Japan). The structural composition of the phosphate ore and the resultant residue was also analyzed using Fourier transform infrared spectroscopy (FT-IR, Thermo Nicolet, USA, 0.5 cm^{-1} resolution). Scanning was conducted on the samples from 4000 cm^{-1} to 400 cm^{-1}. The concentration of P_2O_5 in the liquid phase was measured using an Origin Aquamate 8000 UV-Vis spectrophotometer (Lambda 750S). The particle size distribution of phosphate ore was determined through screening in accordance with ASTM standard, E11.

2.3. Dissolution procedure

Every leaching run occurred within a 200 mL Pyrex three-necked-glass reactor, which was outfitted with a constant speed programmable temperature bath to go on the reaction temperature being stable, fluctuating no more than 0.01 °C throughout the process. Additionally, the agitation action was executed using a digitally mechanical stirrer outfitted with a Teflon rod. The leaching procedure involved adding 200 mL of a freshly prepared hydrochloric acid solution with a particular concentration into the three-necked reactor. All openings of the reactor were sealed, and the temperature bath was heated to the target temperature for 15 min before starting the run. The leaching runs were conducted with the following parameters: agitation speeds (n) set at 50, 100, 200, 300, 400, 500, and 600 rpm; hydrochloric acid concentrations (C_{HCl}) varying from 0.05 to 1.50 N; solid-to-liquid ratios (S/L) ranging from 1/20 to 1/50 g/mL; and leaching temperatures (T) maintained at 14 °C, 20 °C, 25 °C, 30 °C, and 40 °C. At the desired reaction temperature, a specified quantity of crushed phosphate ore (precisely weighed to 0.0001 g) was swiftly introduced into three-necked-glass flask containing 200 mL diluted HCl (leaching agent) at a specific S/L ratio and rotational stirring speed as well. Furthermore, kinetic trials were conducted to assess the dissolution extent of phosphorus ore over time, altering the operational parameters of the reaction.

In the end, the reaction was quit by placing the reactor away from the suction ventilator at the end of the reaction. The solid phase was promptly separated from the suspension using vacuum filtration followed by washing and drying at 105 °C to a constant weight overnight. Washing was done in a triplicate manner with distilled water quantity of one-third the acid volume each time. In this investigation, a batch process approach was implemented, to prevent the error arising from ongoing sampling. Fig. 1 shows the scheme for the system used for the leaching process.

2.4. Evaluations

The phosphate content in an ore is typically indicated by its P_2O_5 amount. The simplest method of quantifying this is through mass measurement, as illustrated in Eq. (5).

$$\mathbf{M}P_2O_5(\%) = \frac{\mathbf{M}P_2O_5}{\mathbf{M}ore} \times 100\% \quad (5)$$

where $\mathbf{M}P_2O_5(\%)$, is the percentage mass of P_2O_5 in the ore; $\mathbf{M}P_2O_5$, is the P_2O_5 mass in the ore; and **M**ore, is the ore total mass.

The percentage dissolution extent of phosphate ore, (D %), is calculated using Eq. (6) as follows:

$$D(\%) = \frac{\mathbf{n}P_2O_4}{\mathbf{M}P_2O_5} \times 100\% \quad (6)$$

Here, $\mathbf{n}P_2O_5$ (gm) refers to the P_2O_5 mass in the aqueous phase.

Based on the calibration curve, the content of P_2O_5 in the aqueous phase can be calculated by (Eq. (7). The absorbance can be subsequently

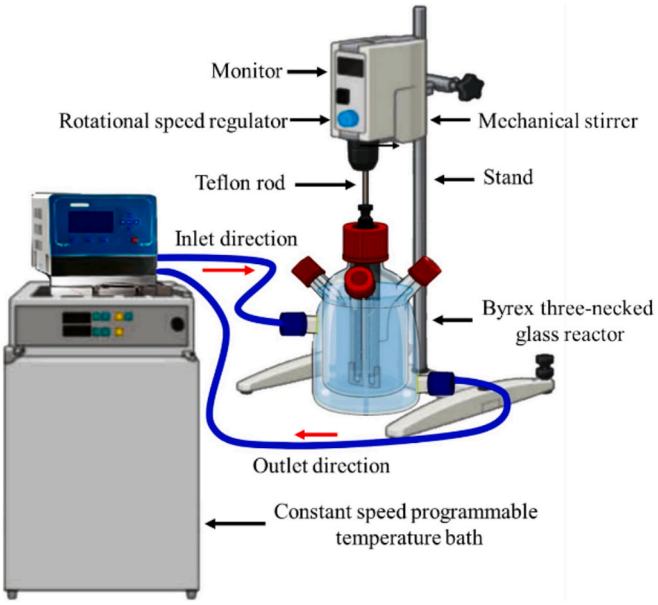

Fig. 1. Schematic diagram of the reaction vessel containing leach liquor connected with digital water bath while mechanical stirring is going on during the kinetic study.

correlated with the phosphate concentration in a linear manner, as demonstrated in supporting info. A1.

$$\mathbf{n}P_2O_5(mg) = \frac{C_{PO_4^{3-}} \times \text{filtrate volume} \times 0.7476}{\text{Sample dilution ratio} \times 10^3} \times 142 \quad (7)$$

The Coefficient of Variation (*CV*) is a statistical metric that indicates the proportion of the standard deviation over the mean of a dataset (Eq. (8), expressed as a percentage as follows:

$$CV(\%) = \frac{\sigma}{\bar{A}} \times 100\% \quad (8)$$

where σ is the standard deviation and $\bar{A}$ is the mean (See supporting info. A2).

3. Results and discussions

3.1. Characterization of phosphate ore

3.1.1. The chemical and phases composition

Chemical analysis as presented in Table 2, reveals that El-Sebaiya phosphorite deposits consist predominantly of CaO, P_2O_5, and SiO_2 in the oxidized phosphorite, with proportions of 40.48 %, 23.05 %, and 14.29 %, respectively. This suggests that the primary component is the apatite mineral.

The diffraction pattern from X-ray of the rock sample demonstrates that the principal mineral components are the Hydroxyfluorapatite ($Ca_5(PO_4)_3$ (OH, F)), Brushite ($CaHPO_4{\cdot}2H_2O$), and Whitlockite (Ca_9 (MgFe) $(PO_4)_6$ (PO_3OH)). These minerals are characterized by prominent diffraction lines with d-spacing of (3.44, 2.72, 2.63, 2.73, 2.81, and 3.46 Å), (7.67, 4.27, 3.06, and 2.68 Å), and (2.47, 2.73, 2.87, and 3.07Å), respectively. The accompanying gangue mineral is predominantly quartz (SiO_2), which is detected at diffraction lines with d-spacing of 3.34, 4.26, 1.82, and 1.54 Å, as illustrated in Fig. 2.

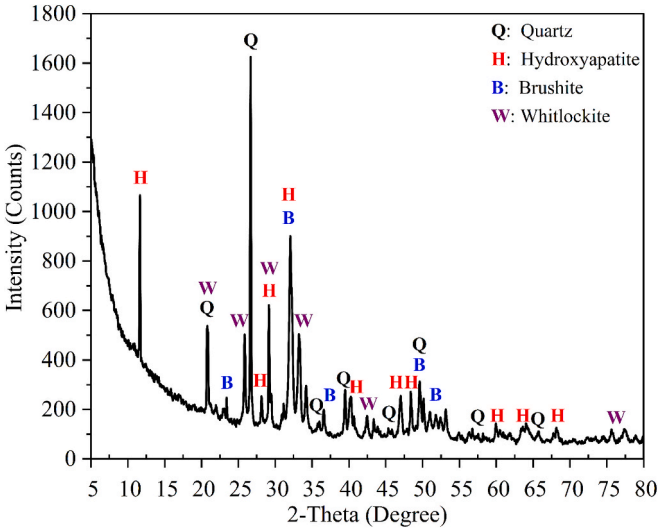

Fig. 2. X-ray diffraction profile of the crushed ore specimen.

3.1.2. The sieve analysis

The phosphate ore was crushed, dried, and subsequently sifted into varying size fractions (+0.063–4.00 mm, +3.00–4.00 mm, +2.00–3.00 mm, +1.00–2.00 mm, +0.50–1.00 mm, +0.25–0.50 mm, +0.20–0.25 mm, +0.15–0.20 mm, +0.075–0.15 mm, +0.063–0.075 mm). Moreover, partition curve was constructed according to plotting the percent partition coefficient for cumulative retained against geometrical mean size of particles as presented in Fig. 3. When a material subjected to sieve analysis, irregular particles exhibit behavior akin to that of a sphere - with an outer diameter that falls within the range of two sieve apertures.

It was shown that the particles of 690 μm in size have an equal probability of being classified as either oversized or undersized; i.e. cut-point of the bulk ore sample (d_{50}) is of 690 μm. On the other hand, 80 % of the bulk sample passed through 2.2 mm opening sieve. Data source for partition curve construction and calculations with screen analysis procedure are demonstrated in supporting info A3.

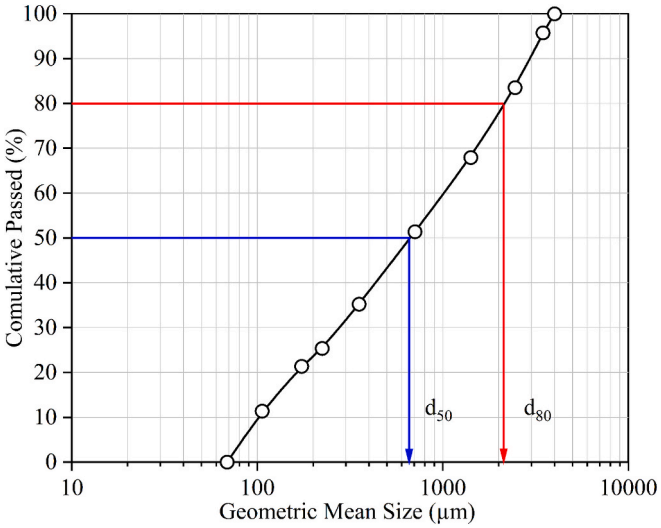

Fig. 3. The particle size distribution (PSD) of the crushed rock sample.

3.2. Impacts of procedural variables on dissolution

3.2.1. The influence of hydrochloric acid concentration on P_2O_5 extraction

An investigation was conducted to analyze the influence of hydrochloric acid concentration (C_{HCl}) on the process of digestion, specifically on the pace at which substances dissolve. The concentrations tested ranged from 0.05 N to 1.50 N. The reaction took place at a temperature of 14 °C (room temperature), with a stirring speed of 400 rpm, a particle size fraction of (+0.063–4.00) mm, and a solid-to-liquid ratio of 1/25 g/mL. Fig. 4 illustrates that a longer leaching period of 320 s leads to a faster and more complete dissolving when higher acid concentrations (e.g., 1.50 N) are used. This results in a significant dissolving of more than 99.9 % of P_2O_5 into the filtrate. The heightened oscillation of H^+ protons when they collide with the outermost layer of an unreacted particle may accounts for this observation. The studies presented by Bandara demonstrate a similar pattern (Bandara and Senanayake, 2015). In the meantime, a regular pattern emerged, with the dissolve rate being very rapid at the outset (usually during the first 30 s) and then gradually decreasing as the leaching duration approached 320 s.

At the 320-second mark, the phosphorus pentoxide recovery percentages were 23.86 %, 31.81 %, 44.60 %, 66.45 %, and 77.95 % for

Table 2
Chemical composition of the studied sample from El-Sebaiya phosphate ore deposit.

Component	L.O.I	F	Na_2O	MgO	Al_2O_3	SiO_2	P_2O_5	SO_3^{-2}	Cl	K_2O	CaO
Weight %	7.66	2.43	0.73	0.42	1.14	14.29	23.05	6.82	0.185	0.074	40.48
Component	TiO_2	V_2O_5	MnO	Fe_2O_3	ZnO	SrO	Y_2O_3	BaO	CeO_2	U	–
Weight %	0.077	0.022	0.11	2.06	0.028	0.176	0.009	0.137	0.093	0.008	–

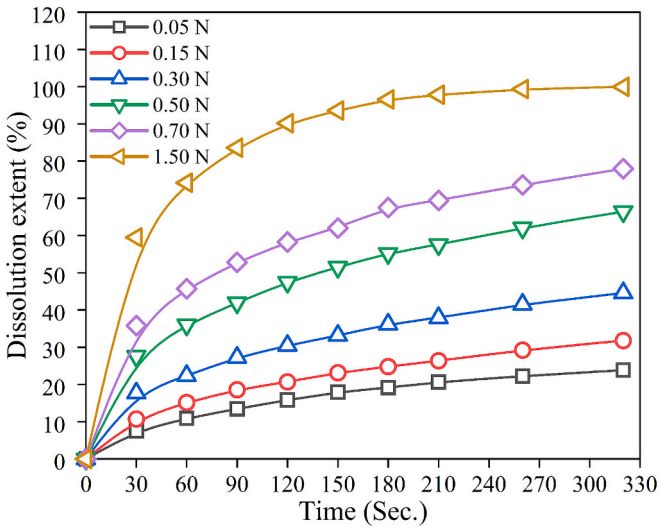

Fig. 4. Effect of HCl concentration on phosphate dissolution extent (S/L = 1/25 g/mL, G = (+0.063–4.00) mm, n = 400 rpm, and T = 14 °C).

solutions with the intermediate concentrations of 0.05 N, 0.15 N, 0.30 N, 0.50 N, and 0.70 N, respectively. At lower concentrations, the solid-to-liquid ratio of 1:25 g/mL utilized in the study may be high, leading to an inadequate amount of acid being administered to the ore sample. Therefore, it is crucial to do research on how the solid-to-liquid (S/L) balance affects the efficiency of leaching the major components. Increasing the acid concentration would result in a significant release of carbon dioxide from the dissolution of carbonates, which would produce foams and significantly increase the use of defoamer. A solution with a hydrochloric acid concentration of 0.70 N was selected for further investigations.

3.2.2. The influence of solid-to-liquid ratio

The impact of the solid-to-liquid ratio (S/L) was investigated through experiments conducted at S/L values of 1/20, 1/25, 1/30, 1/35, 1/40, 1/45 and 1/50 g/mL. Other parameters were held constant, including a particle size of (+0.063–4.00) mm, a stirring speed of 400 rotations per minute, an acid concentration of 0.70 N, and a reaction temperature of 14 °C. Based on Fig. 5, the efficiency of P_2O_5 leaching exhibited a notable initial rise as the ratio decreased. It reached a maximum of around 97.1 % when the liquid-to-solid ratio was 1/50. A reduction in the ore's solid content is predicted to lower its density, which will improve reactant mixing and lessen mass transfer resistance as the reaction proceeds, explaining this phenomenon (Kim et al., 2014). Furthermore, an ideal acid stoichiometry is produced by lowering the concentration of the phosphate ore particles in the reaction mixture. In addition, the dissolution rate difference between 1/50 g/mL and 1/40 g/mL at 320 s is not greater than about 5.55 %. To examine the leaching behavior with particle size modification, a ratio of 1:40 S/L was therefore used.

3.2.3. The influence of particle size

For each of the seven distinct size fractions (+0.063–4.00 mm), (+2.00–4.00 mm), (+1.00–2.00 mm), (+0.50–1.00 mm), (+0.20–0.50 mm), (+0.15–0.20 mm), and (+0.063–0.15 mm), the impact of particle size fractions on the leachability of phosphate ore was investigated. At a stirring speed of 400 rpm, 0.70 N HCl, 14 °C, and S/L ratio of 1/40 g/mL, all these experiments were carried out.

Fig. 6 clearly demonstrates that the dissolving rate of P_2O_5 was higher when the particle size dropped. This can be attributed to the larger surface area and greater freedom of movement of apatite particles. The particle size range of (+0.063–0.15) mm achieved the maximum P_2O_5 extraction rate of 99.93 % after a reaction time of 90 s. As for the rest of the considered size ranges which are: (+0.15–0.20), (+0.20–0.50), (+0.50–1.00), (+1.00–2.00), and (+2.00–4.00) mm, as well as (+0.063–4.0) mm, the dissolution extents obtained after 320 s were 100 %, 96.94 %, 86.64 %, 77.11 %, 73.44 %, and 91.55 %, respectively.

The results show a significant level of agreement with the investigations carried out by Abali et al. (Abali et al., 1997). Since the grinding operation impacts particle size, the Bonds equation states that a high reduction ratio between feed size and product size is connected with increased energy consumption. Table 3 illustrates how the concentration of phosphorus pentoxide fluctuates between different size fractions due to its random liberation during the grinding of phosphate rock. It demonstrates that the high mass % of P_2O_5 exists in (+0.20–0.50) size fraction. Therefore, the following investigations will include the influence of particle size on the leaching process within the specified limits of (+0.20–0.50) mm range.

3.2.4. The influence of agitation rate

During a 320-second reaction time at 14 °C with an HCl concentration of 0.70 N and a solid-to-liquid ratio of 1/40, the effect of stirring

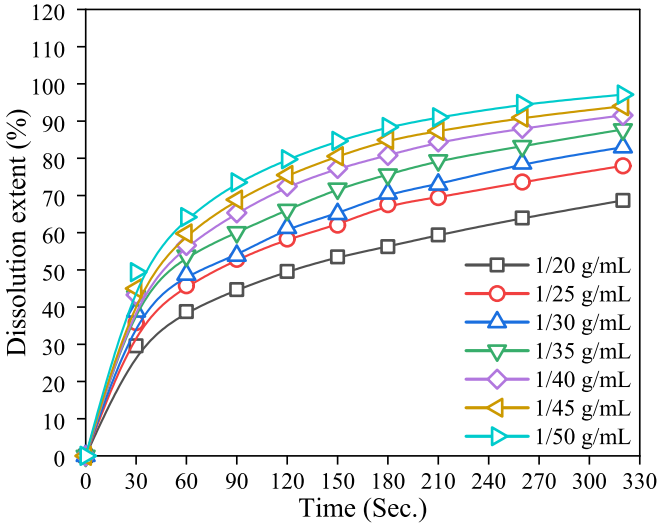

Fig. 5. Effect of solid-to-liquid ratio on P_2O_5 dissolution extent (C_{HCl} = 0.70 N, G = (+0.063–4.00) mm, n = 400 rpm, and T = 14 °C).

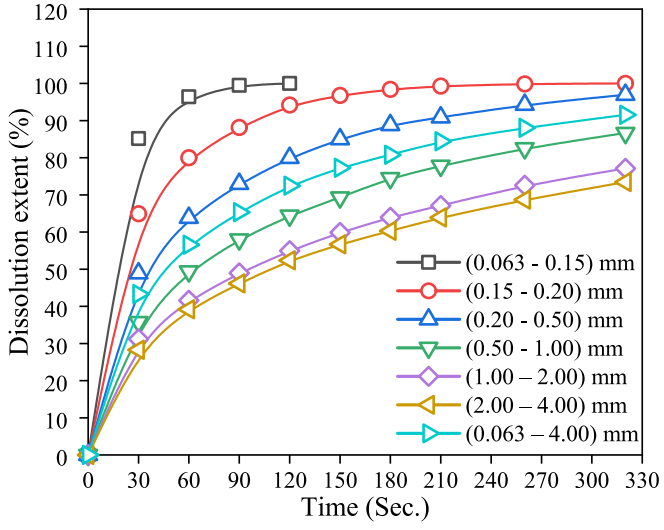

Fig. 6. Effect of particle size fraction on P_2O_5 dissolution extent (C_{HCl} = 0.70 N, S/L = 1/40 g/mL, n = 400 rpm, and T = 14 °C).

Table 3
Chemical composition (mass%, dry basis) and corresponding geometric particle mean size of different fractions of phosphate ore.

Particle size fractions, mm	Geometric mean size (*G*), mm	Yield, %	Mass fraction, %							CaO / P_2O_5
			L.O.I	P_2O_5	CaO	SiO_2	Fe_2O_3	SO_3	Others	
(0.063–0.15)	0.097	21.37	08.28	26.05	38.19	16.23	2.15	5.47	Traces	1.47
(0.15–0.20)	0.173	03.99	08.93	25.49	42.74	10.16	1.91	5.81		1.68
(0.20–0.50)	0.316	26.04	08.70	26.70	43.35	09.65	1.97	4.92		1.62
(0.50–1.00)	0.707	16.54	09.57	25.80	41.76	10.60	2.02	5.44		1.62
(1.00–2.00)	1.414	15.58	07.91	24.58	41.82	12.27	2.09	6.45		1.70
(2.00–4.00)	2.828	16.48	11.27	19.15	33.20	24.23	2.15	5.46		1.73
(0.063–4.00)	0.502	100.0	07.66	23.05	40.48	14.29	2.06	6.82		1.76

speed (*n*) on the rate of phosphate ore dissolution was investigated. As evidenced by the percentage of P_2O_5 recovery, Fig. 7 describes how the speed of agitation affects the amount of phosphate ore digestion.

Increasing the stirring speed and reaction duration clearly increased the P_2O_5 leaching percentage, indicating improved leaching performance under intensified hydrodynamic conditions. When the stirring rate is 300 rpm or lower, the leaching agents may not effectively penetrate the particles' surfaces suggesting that the process is predominantly controlled by external mass transfer through the liquid film. The inadequate stirring fails to fully suspend the particles. This leads to the inadequate transport of hydrogen ions (H^+) from the bulk solution to the surface of the ore particles, as well as the delayed removal of reaction products back into the solution.

In contrast, when the speed surpasses 400 rpm, the leaching efficiency curves at 400, 500, and 600 rpm exhibit a tendency to converge. There is no significant improvement in the particle dissolution rate, particularly if the particles are already completely suspended. The results indicated that the maximum recovery rates of phosphorus pentoxide content during the reaction time period when using the latter stirring speeds were 91.55 %, 92.25 %, and 93.92 %, respectively. Additionally, swirling the leaching acid solution reduces exterior diffusion resistance (Calmanovici et al., 1997). As a result, the external diffusion resistance was minimized and the leaching kinetics become increasingly governed by surface chemical reactions occurring at the ore-solution interface. This transition elucidates the observed plateau in leaching efficiency at elevated stirring speeds, where additional increases in mixing intensity cease to facilitate dissolution.

These findings point to a mechanistic transition in the rate-controlling step. Thus, the apparent contradiction is reconciled by recognizing that the dissolution process does not follow a single controlling mechanism, but rather evolves from an initial mass transfer-limited regime to one dominated by interfacial reaction kinetics under optimized hydrodynamic conditions. Hence, an agitation rate of 400 rpm ensures sufficient particle suspension and has been approved for subsequent trials.

3.2.5. *The influence of reaction temperature*

To determine how temperature affects P_2O_5 leaching efficiency, 400 rotations per minute, size fraction of (+0.2–0.5) mm, 1/40 *S/L* ratio, and 0.70 N HCl acid concentration were used in a series of tests at temperatures ranging from 14 °C to 40 °C. The kinetic isotherms that were obtained are depicted in Fig. 8. It is true that the higher temperature slightly affected the rate at which P_2O_5 recovered.

The digestion recovery shows a rapid increase in the initial phase of the process, where the recovery rose from 72.47 % to 83.76 % within the first 120 s as the temperature increased from 14 °C to 40 °C. This significant improvement suggests that temperature has a strong influence on the early kinetics of the reaction, which is typical when surface reaction controls the process. However, from 120 s to 320 s, despite the temperature remaining constant at 40 °C, the recovery increased only marginally from 83.76 % to 98.03 %. Notably, at 25 °C, recovery was already close to 95.37 %, indicating that most of the leaching occurred at a lower temperature, and the higher temperature only contributed a small gain of 2.66 %.

In case of diffusion-controlled processes, increasing the temperature does not accelerate the speed of molecular movement in the leaching suspension, the frequency of collisions, the rate at which mass is transferred, or the reaction rate between the leaching agent and the mineral particles(Liao et al., 2015; Rao et al., 2015). Habashi' s observation indicates that the leaching process is mostly controlled by diffusion, with just a tiny correlation to temperature. Conversely, temperature fluctuations greatly affect a chemically controlled process (Habashi,

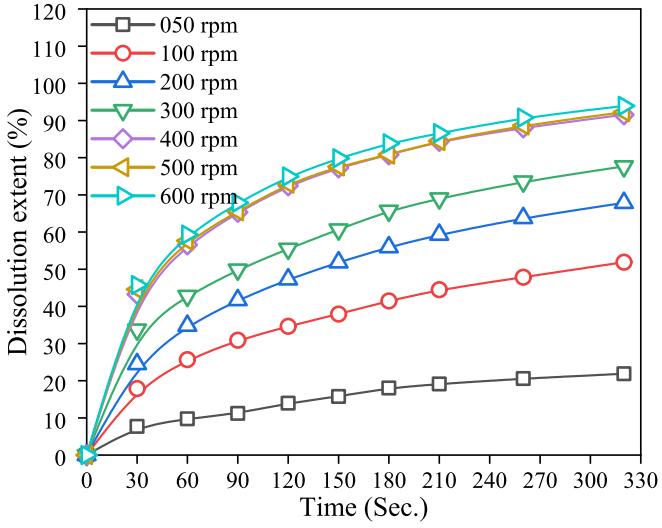

Fig. 7. Effect of stirring rate on P_2O_5 dissolution extent (C_{HCl} = 0.70 N, *S/L* = 1/40 g/mL, *G*=(+0.20–0.50) mm, and *T* = 14 °C).

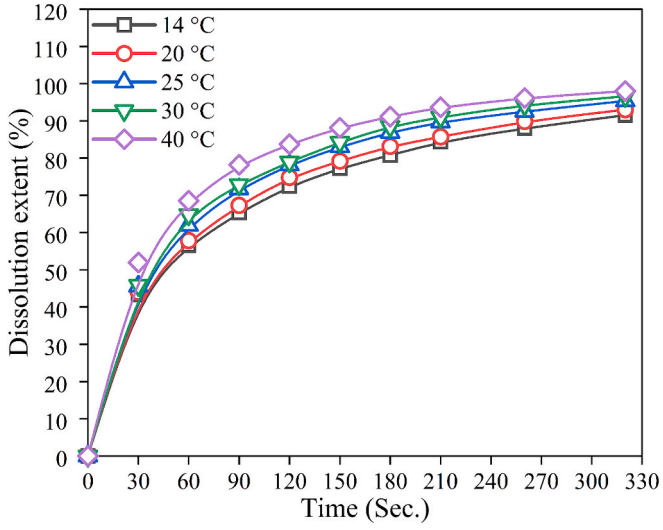

Fig. 8. Effect of reaction temperature on P_2O_5 dissolution extent (C_{HCl} = 0.70 N, *S/L* = 1/40 g/mL, *G*=(+0.20–0.50) mm, and *n* = 400 rpm).

2017). The dissolution kinetics show a two-stage mechanism:

a) The sharp recovery rise with temperature increase in the early stage suggests that the reaction is initially controlled by a temperature-sensitive mechanism (chemical reaction control).
b) The flattening of the recovery curve at constant temperature (from 120 s onward) implies that the rate slows down despite constant thermal energy input. This typically indicates a shift to a diffusion-controlled process. As the reaction progresses, the formation of a diffusion barrier (pores network) leads to a shift toward a diffusion-controlled process (intraparticle diffusion), where temperature has limited additional effect.

Consequently, it is recommended to use hydrochloric acid to extract phosphorus pentoxide from phosphate rock at a temperature lower than 30 °C. Leaching at that temperature serves the dual purpose of preventing equipment corrosion and saving energy.

3.3. Meeting the optimum leaching conditions

The leaching results of phosphate ore in multiple acidic solutions, as documented in the literature and our investigation, are described in Table 4. The leaching efficiency exhibited considerable variation based on the distinct compositions, structures, and leaching conditions of various phosphate ores. Despite these considerations, this study demonstrates superior leaching efficiency under mild conditions (low temperature, short time, moderate acid strength), which is highly promising from both economic and environmental perspectives. This could indicate favorable ore mineralogy and particle size, well-optimized agitation and acid concentration, and finally kinetically efficient leaching system likely governed by surface reaction control at the specified particle size, due to excellent performance in such a short time.

To optimize the phosphate leaching process using either acid, several conditions must be met:

- Ore Characterization: Conducting a thorough analysis of the phosphate ore to determine its composition, including the presence of impurities and valuable by-products, to select the most suitable leaching agent (Guan et al., 2022).
- Process Optimization: Adjusting parameters such as acid concentration, solid/liquid ratio, particle size, stirring speed, temperature, and leaching time to maximize phosphate recovery while minimizing reagent consumption and operational costs (Gharabaghi et al., 2010).
- Material Selection: Using corrosion-resistant materials in equipment design to withstand the acidic environment and ensure operational longevity.
- Environmental Compliance: Implementation measures to manage and treat waste products, ensuring adherence to environmental regulations and minimizing ecological impact (Tayibi et al., 2009).
- Economic Assessment: Conducting a comprehensive cost-benefit analysis considering factors like grinding cost, acid cost, potential revenue from by-products, and infrastructure requirements to determine the most economically advantageous method (Campbell et al., 2023).

3.4. Kinetic analysis

The dissolution of phosphate ore in a hydrochloric acid solution entails a chemical reaction between a solid and a liquid. This process can be characterized as a heterogeneous reaction, in which the ore particles interact with the leaching agent. When a system consists of various components, the total rate expression becomes intricate due to the interplay between physical and chemical processes. The whole response model is stated as follows(Sohn, 1979):

$$R_a + cR_b = P \tag{9}$$

The equation uses the symbol "R_a" to denote the liquid employed for leaching, "R_b" to signify the solid reactants, which are the ore particles, "c" to indicate the stoichiometric coefficient, and "P" to refer to the resultant product. Furthermore, it is presumed that the particles participating in the reaction possess a spherical geometry and maintain an equal size.

A hypothesized series of reactions has been suggested to clarify how

Table 4
Comparison of the leaching behaviors of several phosphate ores from our investigation with existing literature*.

Origin	P_2O_5 (in ore) %	Leaching		Agitation rate, rpm	Particle size range, μm	Acid concentration	S/L ratio	Temp., °C	D, %	Remarks	Ref.
		Agent	Time, Sec								
China	28.11	HCl	240	300	150–180	0.488 M	1/250	30	97.80		(Lv et al., 2021)
Turkey	16.58	H_2SO_4	900	2513	710–860	98 % w/w	1/40	70	99.98		(Sevim et al., 2003)
Nigeria	33.81	HNO_3	2400	400	−100	13.3 M	1/100	70	100.0		(Olanipekun, 2003)
Egypt	30.1	HCl	960	400	63–150	0.1 M	1/1500	50	80.45		(Azeez et al., 2024)
Pakistan	22.7	HCl	–	***a***	74–208	3.5 %	1/15	***b***	98.15		(Zafar et al., 2006)
Nigeria	33.1	H_2SO_4/ HCl	1800	500	−53	H_2SO_4:HCl (5.5 M:2.4 M)	1/50	90	92.00	H_2SO_4: HCl = 1:1	(Ethiopia, 1999)
		H_2SO_4	1800	500	−53	5.5 M	1/50	90	79.00		
China	36.54 ± 0.3	H_3PO_4	1200	400	59–260	30 wt%	1/10	70	100.0		(Liao et al., 2023)
Turkey	24.56	SO_2-Saturated water	1800	1885	1400–1700	–	1/67	15	100.0		(Yartaşi et al., 1994)
Nigeria	35–40	HNO_3	±1000	500	–	1 M	1/250	60	100.0		(Poissonnier et al., 2021)
	30–35	HNO_3	120	500	–	0.1 M	1/250	60	100.0		
China	31.7	HCl	7200	150	–	36 %	1/2.2	60	98.80		(Seyed Ghasemi and Azizi, 2018)
Turkey	22.6	Cl_2 gas in water	5400	400	180–250	Cl_2 flow rate = 300 mL/min	1/150	20	98.65		(Abali et al., 1997)
Egypt	26.05	HCl	90	400	63–150	0.7 N	1/40	14	99.93		This work

*: Moderate rotational speed = 150–300 rpm, ***b***: Ambient temperature.

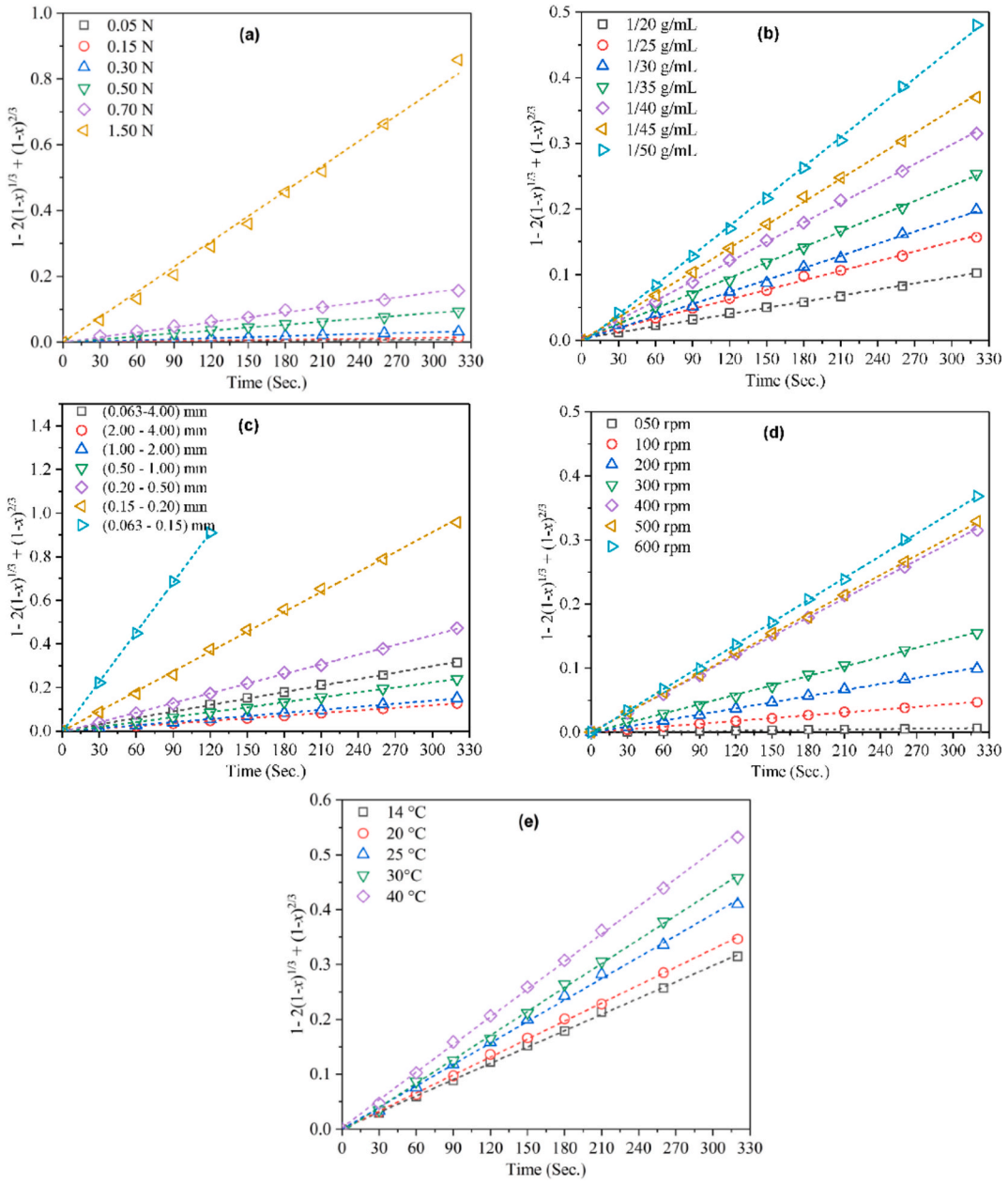

Fig. 9. Plot of $[1–2(1\text{-}x)^{1/3}+(1\text{-}x)^{2/3}]$ vs. time for P_2O_5 dissolution rate-influencing parameters: a) HCl acid concentration, b) solid-to-liquid ratio, c) stirring speed, d) particle size, e) reaction temperature.

fluorapatite dissolves in hydrochloric acid(Dorozhkin, 1997):

$$Ca_5(PO_4)_3F + 7H^+ = 5Ca^{2+} + 3(H_2PO_4)^- + HF \quad (10)$$

$$Ca_5(PO_4)_3F + H_2O + H^+ = Ca_5(PO_4)_3 \bullet H_2O + HF \quad (11)$$

$$Ca_5(PO_4)_3 \bullet H_2O = 3Ca_3(PO_4)_2 + Ca^{2+} + 2H_2O + 2e^- \quad (12)$$

$$Ca_3(PO_4)_2 + 2H^+ = CaHPO_4 + Ca^{2+} \quad (13)$$

$$CaHPO_4 = Ca^{2+} + (HPO_4)^- \quad (14)$$

$$CaHPO_4 + 2H^+ = Ca^{2+} + H_3PO_4 \quad (15)$$

Employing the previously outlined reactions as a basis, the influences of acid concentration, liquid-to-solid ratio, particle size fraction, agitation rate, and temperature on the kinetics and mechanism of phosphorus pentoxide (P_2O_5) extraction in a hydrochloric acid (HCl) solution are scrutinized and appraised.

Considering the ore mostly consists of densely packed visible grains, which gradually decrease in size when a layer forms around the unreacted core during leaching (as depicted in Fig. 14), the research has opted for the shrinking core model. This type is more appropriate for the leaching process of solids that lack pores. The dissolution mechanism is thought to involve the following four processes, which are thought to happen in order:

1. Diffusion of the leaching agent through the thin film layer around the particle,
2. Surface chemical reaction within the unreacted core at the interface, along with,
3. Leaching agent diffusion through the pore network,
4. Getting all the soluble products out of the reaction site by passing them through the product layer and the aqueous thin film toward the liquid's bulk.

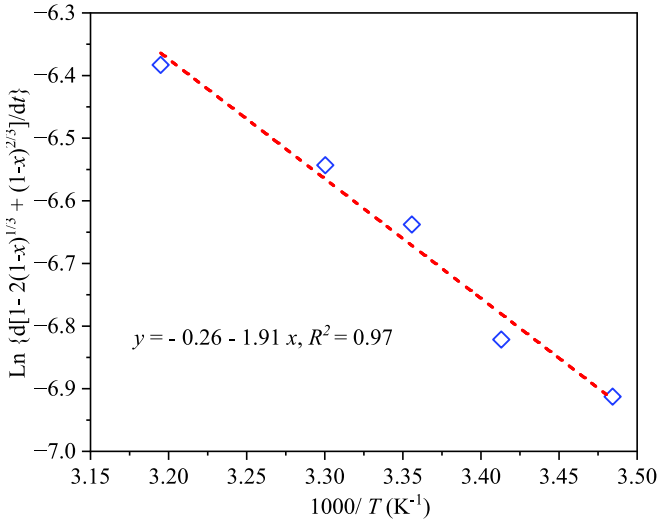

Fig. 10. Arrhenius plot for phosphate rock dissolution.

3.4.1. *Model fitting*

Various Shrinking Core Models (SCMs) were applied to the experimental data to identify the step that controls the rate of the leaching process and to gain a deeper insight into its behavior. To achieve this, the following mathematical formulations were employed to elucidate the dissolution kinetics of P_2O_5 Eqs. (16–19). If the leaching kinetics are dictated by surface chemical reactions, liquid film diffusion, ash layer diffusion, or a combination thereof in a mixed kinetic model(Espiari et al., 2006; Seyed Ghasemi and Azizi, 2018), the integrated rate model k_P, k_S, k_L, and k_M are being referred to respectively.

$$1-(1-x)^{1/3}=k_P.t \tag{16}$$

$$1-(1-x)^{2/3}=k_S.t \tag{17}$$

$$1+2(1-x)-3(1-x)^{2/3}=k_L.t \tag{18}$$

$$1-(1-x)^{2/3}+2(1-x)^{1/3}=k_M.t \tag{19}$$

The framework utilize the term "x" to denote the fractional conversion of P_2O_5 within a restricted range ($0 \leq x < 1$). The variable "t" represents the time it takes for the reaction to occur, measured in seconds. Additionally, "k_P", "k_S", "k_L", and "k_M" are used to designate the apparent rate constants that govern surface chemical reactions, liquid film diffusion, ash or product layer diffusion, and a mixed kinetic model, respectively. These rate constants are expressed in units of sec^{-1}. When analyzing mechanisms of reaction employing kinetic approaches, it is generally advisable to acquire five rate coefficients with an error rate of ±5 % rather than a single fixed with a certainty of ±1 %. The analysis of the experimental results, utilizing graphical and statistical techniques within the framework of fluid–solid mixed reaction mathematical models, concluded that the data adhered to a mixed controlled kinetic model. The supporting information presents Table A3, which displays the data from the kinetic investigations, including the rate constants and their corresponding regression coefficients for various kinetic models as influenced by the leaching variables under investigation.

Curves were generated by plotting conversion fraction values against SCMs at preset time intervals to represent the dissolving process. Conversely, the mixed mechanism model produced distinct linear patterns intersecting at zero for each leaching parameter, suggesting that the rate of digestion might be controlled by both chemical reaction and

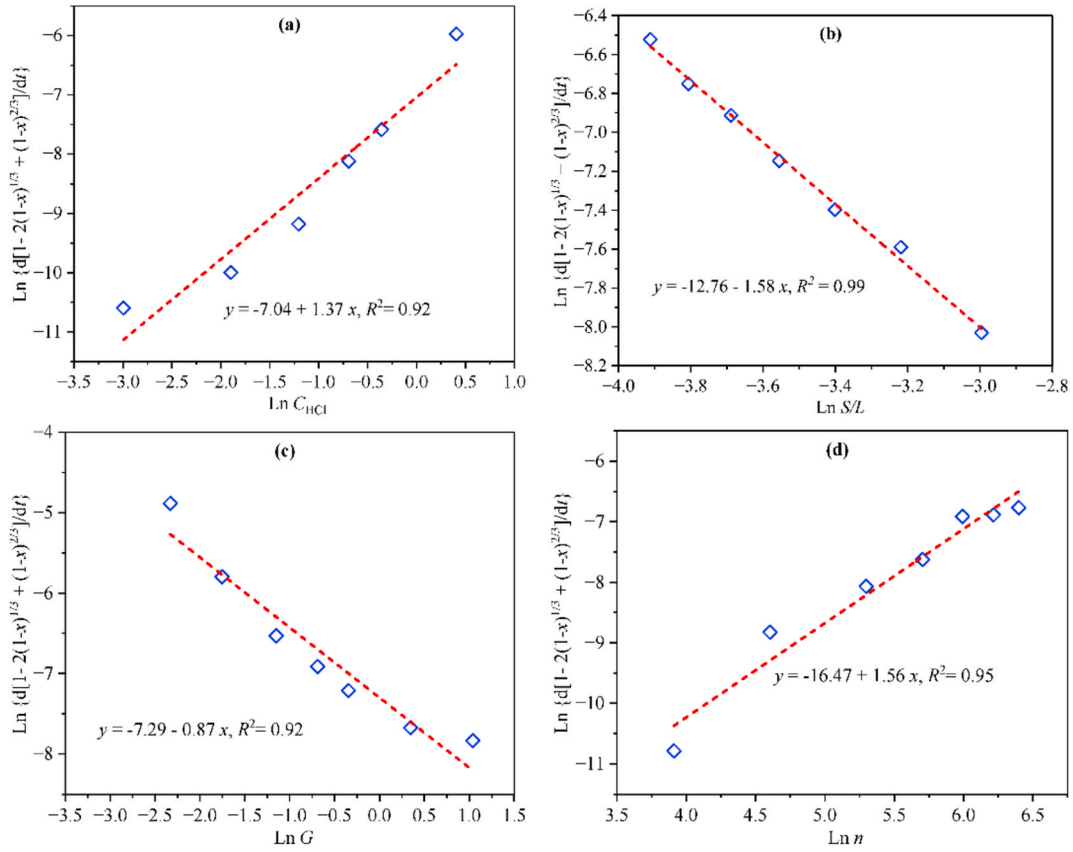

Fig. 11. Plot of Ln [d[1–2(1-x)$^{1/3}$+(1-x)$^{2/3}$]/dt] for influential parameters on P_2O_5 dissolution rate against natural logarithm of: a) HCl acid concentration, b) solid-to-liquid ratio, c) stirring speed, d) particle size.

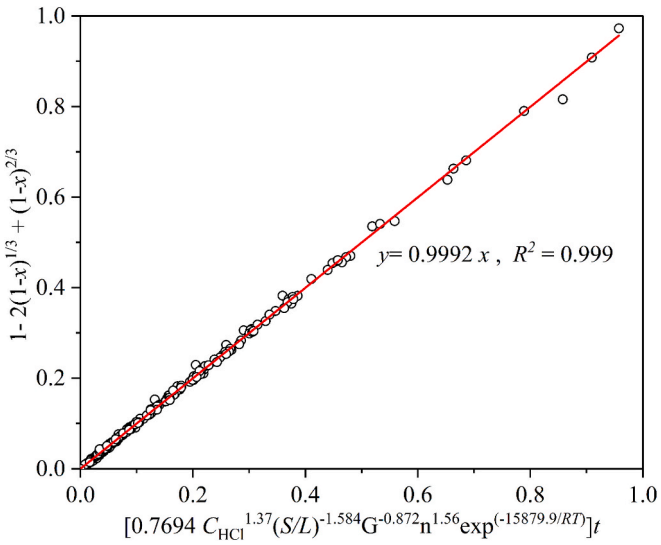

Fig. 12. Comparison between the empirical kinetic model and experimental values of $1–2(1\text{-}x)^{1/3}+(1\text{-}x)^{2/3}$ for P_2O_5 dissolution rate.

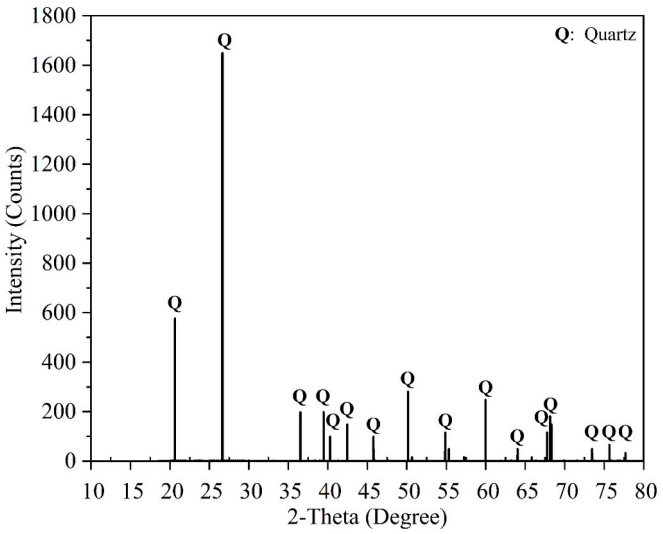

Fig. 14. X-ray diffraction pattern of the residue specimen at optimum condition.

diffusion mechanisms. The apparent rate constants and R^2 were determined by graphing the expression "$1\text{-}2(1\text{-}x)^{1/3}+(1\text{-}x)^{2/3}$" against "$t$" for each parameter, as shown in Fig. 9 for the mixed kinetic model. The apparent rate constants in these figures have been identified based on the gradients of the linear regressions.

3.4.2. Rate-controlling step of the leaching kinetics

It is of the utmost importance to determine the rate-controlling phase of the leaching process. This can be accomplished by confirming that the kinetic parameters that have been measured, such as the order of reaction or activation energy, agree with the mechanism that has been posited (Crundwell, 2013; Madakkaruppan et al., 2016). Therefore, the Arrhenius equation was utilized to calculate the apparent activation energy and gain a more precise understanding of the mechanism and kinetics of the process. The relationship between the reaction rate and temperature follows the Arrhenius-type equation (Eq. 20 or 21).

$$k = A.exp^{(-Ea/RT)} \tag{20}$$

$$\ln k = \ln A - Ea/RT \tag{21}$$

In this context, Ea denotes the apparent activation energy (J/mol), k signifies the reaction rate constant (sec^{-1}), A represents the frequency factor (sec^{-1}), T stands for the reaction temperature measured in Kelvin (K), and R is the universal gas constant valued at 8.314 J/(mol K).

The Arrhenius equation was graphed by plotting $\text{Ln}\{d[1–2(1\text{-}x)^{1/3}+(1\text{-}x)^{2/3}]/dt\}$ against $1/T \times 10^3$ (refer to Fig. 10) for each temperature.

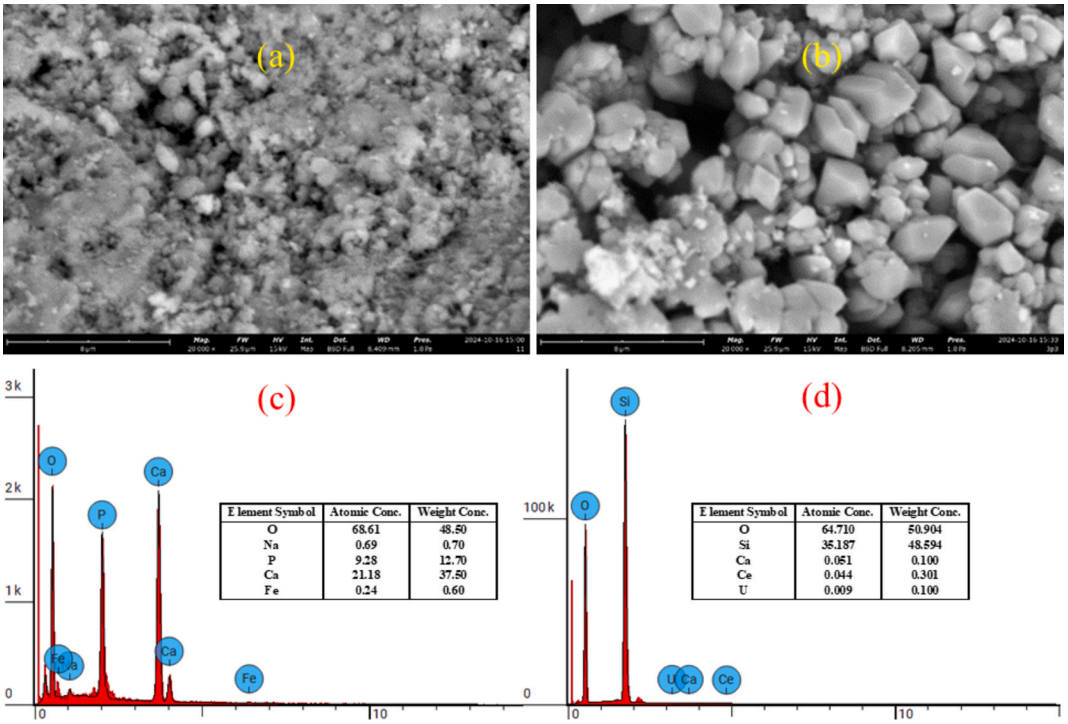

Fig. 13. SEM images of (a) ore grains, and (b) residues after leaching (t = 90 sec at 14 °C, size fraction of (+0.063–0.15) mm, S/L ratio of 1/40, 400 rpm, and 0.70 N HCl). EDS analysis of (c) ore grains, and (d) residue grains.

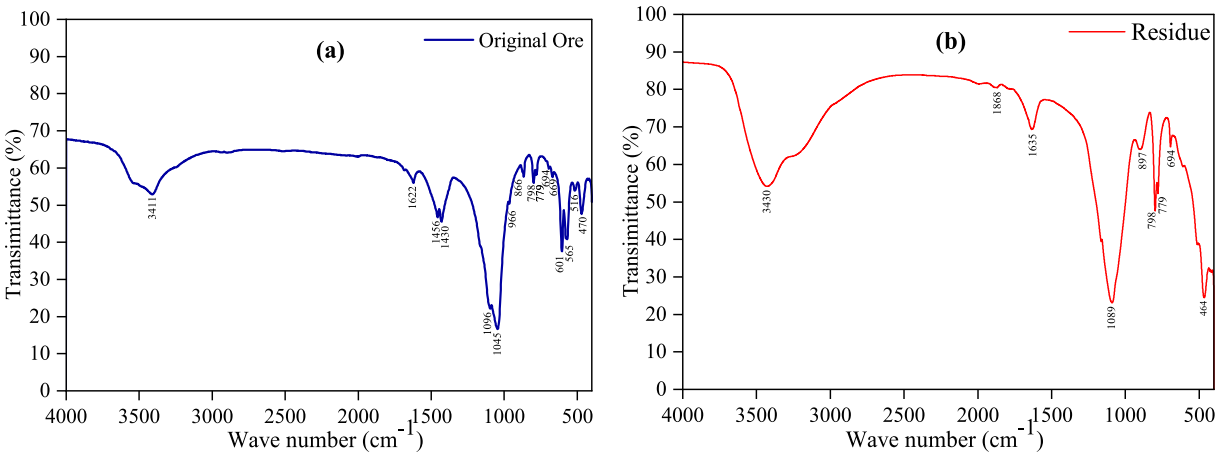

Fig. 15. FTIR analysis for a) original phosphate ore, and b) final residue.

The activation energy was then determined by calculating the slope of the straight line, where the slope is equal to the negative activation energy divided by the gas constant ($-Ea/R$). From this graph, the activation energy for phosphate dissolution in hydrochloric acid within the temperature range of (14–40)°C is determined to be 15.88 kJ/mol for the interval of (0–320) seconds.

Since, diffusion-controlled processes often have lower activation energies, typically around 21 kJ/mol (Jung and Mishra, 2016; Liu et al., 2012), whereas chemical-controlled processes frequently have energies around 40 kJ/mol (Seyed Ghasemi and Azizi, 2018). In addition, in a process regulated by mixed control, the activation energy approximately ranges from 21 to 42 kJ/mol (Liu et al., 2012).The results shown here are inconsistent with the notion that a mixed model regulates the rate-controlling step. Despite the mixed kinetic model showing the highest fitness on the leaching data and the dissolution rate being influenced by both diffusion and chemical reaction processes, it can be inferred from the activation energy magnitude (15.88 kJ/mol) that the primary mechanism governing the leaching kinetics is diffusion via pores. The presence of numerous patterns that govern the entire phenomenon is responsible for this paradox, which arises from the extensive variation in the size range of particles. This dual behavior likely results from sample heterogeneity, where smaller particles, due to their higher surface area, undergo chemical reaction-controlled leaching, while larger particles face diffusion limitations as the leaching agent must penetrate their internal structure. The first assumption, based on the *CV* of a magnitude exceeding 30 %, indicates a wide size distribution; the bigger particles were not yet dissolved during the leaching, but there was thought to be a point when the smaller particles were fully leached (Gbor and Jia, 2004). The *CV* value of the typical sample was calculated to be 112 %. Second, the chemical reaction may initially control the process, but no layer of product forms as the reaction progresses. Thus, the pores may resist the leaching agent's penetration, reaching a point where the diffusion rate through the product layer matches the rate of the chemical reaction due to the effect of continuous agitation (Faraji et al., 2022).

3.4.3. Reaction orders with respect to leaching parameters

Fig. 11 (a), (b), (c), and (d) show graphs of the natural logarithm of the derivative of the expression $[1–2(1\text{-}x)^{1/3} + (1\text{-}x)^{2/3}]$ with respect to time, plotted against Ln C_{HCl}, Ln S/L, ln G, and Ln n, respectively. The semi-empirical kinetic equation (Eq. (22)) describes the process of P_2O_5 leaching during the entire reaction duration.

$$AC_{HCl}^{\propto}(S/L)^{\beta}G^{\gamma}n^{\varepsilon}exp^{(-Ea/RT)}t \tag{22}$$

The power variables α, β, ϒ, and ε denote the reaction order for their base parameters. The magnitude of these constants gained from the slope of the straight lines resulted from the graphs of Ln $[d[1–2(1\text{-}x)^{1/3}+(1\text{-}x)^{2/3}]/dt]$ versus Ln C_{HCl}, Ln S/L, ln G, and Ln n, respectively. Lastly, (Eq. (23)) provides the reaction kinetic model for extracting P_2O_5 from the phosphate ore deposit using hydrochloric acid reagent:

$$1-2(1-x)^{1/3}+(1-x)^{2/3} = [0.7694C_{HCl}^{1.37}(S/L)^{-1.584}G^{-0.872}n^{1.56}exp^{(-15879.9/RT)}]t \tag{23}$$

The study revealed that the reaction rate exhibited a direct proportionality to the initial acid concentration raised to the power of 1.37 and stirring speed raised to the power of 1.56, and an inverse proportionality to both of solid-to-liquid ratio and particle size raised to the power of 1.58 and 0.87, respectively. The pre-exponential factor (A) was determined to be 0.7694 sec^{-1} using Eq. (15). Therefore, the rate of reaction is directly proportional to the concentration of acid $[H^+]$, following a first-order dependence.

The relationship between reaction kinetics and particle size arises when the rate of the reaction is regulated by diffusion through a layer of product. In this scenario, the diffusion rate is consistently proportional to the reciprocal of the starting particle radius, following an inverse square relationship. On the other hand, for reactions controlled by a chemical reaction, the leaching kinetics vary inversely with the initial particle radius (Dreisinger and Abed, 2002).

The graph depicted in Fig. 12 presents a comparison between the experimental conversion values ($X_{exp} = [0.7694C_{HCl}^{1.37}(S/L)^{-1.584}G^{-0.872}n^{1.56}\exp^{(-15879.9/RT)}]t$) and the calculated values ($X_{cal} = 1–2(1\text{-}x)^{1/3}+(1\text{-}x)^{2/3}$) derived from the preceding Eq. (18). It can be deduced that the agreement is acceptable.

4. Physicochemical characterizations of the optimum residue

Images obtained via scanning electron microscopy (SEM) of the phosphate sample prior to and subsequent to leaching with HCl solution (t = 90 s at 14 °C, size fraction of (+0.063–0.15) mm, solid-to-liquid ratio of 1/40, 400 rpm, and 0.70 N HCl) were recorded and shown in Fig. 13. The SEM images presented in Fig. 13 (a, b) indicate that the morphology of the phosphate sample has undergone progressive alterations upon leaching. The SEM image of the phosphate sample prior to leaching (Fig. 13a) revealed a smooth surface with aggregation resulting from the presence of diverse phosphate components. Nonetheless, the structure of the residue post-HCl leaching (Fig. 13b) has altered, revealing distinct silicon particles. This indicates that all minerals encasing the silicon and occupying its micro pores have been dissolved. Energy dispersive X-ray spectroscopy (EDS) of the phosphate sample prior to leaching (Fig. 13c) identifies the presence of O, Fe, Na, Ca, and P in significant amounts. However, no phosphorus was detected in the residue following leaching with hydrochloric acid (Fig. 13d), and the concentrations of most elements were greatly diminished, which may be

attributed to a complete phosphate dissolution. This result was confirmed by XRD analysis of the residue sample as demonstrated in Fig. 14.

Fig. 15 displays the FTIR spectrum of the original phosphate ore and its residue after the leaching process. Fig. 15a indicated that the phosphate group displays the most prominent IR peaks, occurring at 1045 and 604 cm^{-1}, due to asymmetric stretching and bending vibrations of P–O bonds, respectively. Si–O bonds depict characteristic peaks at 1096, 798, and 470 cm^{-1}. The Si–O stretching vibration mode at 1096 cm^{-1} overlaps with the P-O peak. The stretching band of calcium carbonate, $\nu(CO_3)$, is seen at around 1430–1460 cm^{-1}. The wide characteristic peak in the range of 3600–3400 cm^{-1} could be attributed to the –OH stretching vibration of adsorbed water and bound water molecules.

After the leaching process, the characteristic IR peaks of PO_4^{3-} group completely disappeared indicating the complete dissolving of the phosphorus-containing moieties (Fig. 15 b). The spectra instead showed characteristic peaks of Si–O functional groups as the main residual component. IR peaks corresponding to adsorbed water molecules become more intense as a result of the leaching process.

5. Conclusions

The influence of process variables on the dissolution reaction indicated that the extent of phosphate ore dissolving markedly increased with higher concentrations of hydrochloric acid and stirring rates, alongside a reduction in the particle size of the phosphate ore as well as solid-to-liquid ratios and gently with reaction temperatures. At an equivalent temperature and stirring speed, nearly complete recovery of phosphorus pentoxide was attained when the initial sample was subjected to 1.5 N HCl at a solid-to-liquid ratio of 1:25 for approximately 320 s, whereas a comparable recovery percentage was observed when the size fraction (+0.063–0.15) mm was treated with 0.7 N HCl at a solid-to-liquid ratio of 1:40 for a duration of 90 s.

The leaching rate demonstrated an inverse relationship with particle size but did not fully align with standard chemical reaction control or diffusion control models. A mixed-model approach was utilized, suggesting that both chemical reaction kinetics and diffusion limitations contribute to the leaching process. The typical sample had an estimated variance coefficient of 112 %.

The mathematical analysis of the results yields an activation energy of 15.88 kJ mol^{-1} along with a semi empirical formula as follows:

$$1-2(1-x)^{1/3}+(1-x)^{2/3} = [0.7694C_{HCl}^{1.37}(S/L)^{-1.584}G^{-0.872}n^{1.56}exp^{(-15879.9/RT)}]t$$

SEM images show phosphate sample morphology changes post-leaching, with distinct silica particles indicating dissolution of minerals encasing silicon as well as in micro pores, contrasting with the smooth surface before leaching. EDS reveals no significant amounts of phosphorus was detected, indicating complete phosphate dissolution. XRD and FT-IR analyses confirmed that the residue sample includes only SiO_2 as the main phase.

Associated content

The Supporting Information that is available. Methodology and derivations for UV/Vis analysis, steps to calculate the coefficient of variation, data source for partition curve construction and calculations with screen analysis procedure, and kinetic investigation results corresponds to the fractional recovery of the actual leaching parameters (PDF).

CRediT authorship contribution statement

Hassan H.A. Younes: Writing – original draft, Methodology, Formal analysis, Data curation. **Lei Qin:** Software, Formal analysis. **Abdelaal S. A. Ahmed:** Formal analysis, Conceptualization. **Feifei Jia:** Resources, Methodology. **Shaoxian Song:** Validation, Supervision. **Weiquan Zhan:** Writing – review & editing, Methodology.

Declaration of competing interest

The authors declare that they have no known competing financial interests or personal relationships that could have appeared to influence the work reported in this paper.

Appendix A. Supplementary material

Supplementary data to this article can be found online at https://doi.org/10.1016/j.mineng.2025.109480.

Data availability

Data will be made available on request.

References

Abali, Y., Çolak, S., Yartaşi, A., 1997. Dissolution kinetics of phosphate rock with Cl_2 gas in water. Hydrometall. 46, 13–25. https://doi.org/10.1016/S0304-386X(96)00094-1.

Abdel-Aal, E.S.A., 2000. Recovery of phosphoric acid from Egyptian Nile Valley phosphate tailings. Miner. Eng. 13, 223–226. https://doi.org/10.1016/S0892-6875(99)00168-5.

Abouzeid, A.Z.M., 2008. Physical and thermal treatment of phosphate ores — an overview. Int. J. Miner. Process. 85, 59–84. https://doi.org/10.1016/J.MINPRO.2007.09.001.

Aly, H.F., Ali, M.M., Taha, M.H., 2013. Dissolution kinetics of Western Desert phosphate rocks, Abu Tartur with hydrochloric acid dissolution kinetics of Western Deseret Phosphate Rocks, Abu Tartur with hydrochloric acid. Arab J. Nucl. Sci. Appl. 46, 1–16.

Antar, K., Jemal, M., 2008. Kinetics and thermodynamics of the attack of a phosphate ore by acid solutions at different temperatures. Thermochim Acta 474, 32–35. https://doi.org/10.1016/J.TCA.2008.05.006.

Arroug, L., Elaatmani, M., Zegzouti, A., Aitbabram, M., 2021. Low-grade phosphate tailings beneficiation via organic acid leaching: process optimization and kinetic studies. Minerals 11, 492. https://doi.org/10.3390/MIN11050492.

Ashraf, M., Zafar, Z.I., Ansari, T.M., 2005. Selective leaching kinetics and upgrading of low-grade calcareous phosphate rock in succinic acid. Hydrometall. 80, 286–292. https://doi.org/10.1016/J.HYDROMET.2005.09.001.

Ayinla, K.I., Baba, Oyinloye, Olaoluwa, D.T., Ibrahim, Raji, Abdulrahman, Ajetomobi, O. O., 2018. Establishment of Dissolution Kinetics and Mechanism of Direct Leaching of Gagi Phosphate Rock in Hydrochloric Acid Solution. AJPAS J. 6, 1–10.

Azeez, R.S., Tõnsuaadu, K., Kaljuvee, T., Trikkel, A., 2024. Kinetics of Estonian phosphate rock dissolution in hydrochloric acid. Minerals 14, 322. https://doi.org/10.3390/MIN14030322.

Bandara, A.M.T.S., Senanayake, G., 2019. Dissolution of calcium, phosphate, fluoride and rare earth elements (REEs) from a disc of natural fluorapatite mineral (FAP) in perchloric, hydrochloric, nitric, sulphuric and phosphoric acid solutions: a kinetic model and comparative batch leaching of major and minor elements from FAP and RE-FAP concentrate. Hydrometall. 184, 218–236. https://doi.org/10.1016/J.HYDROMET.2018.09.002.

Bandara, A.M.T.S., Senanayake, G., 2015. Leachability of rare-earth, calcium and minor metal ions from natural fluorapatite in perchloric, hydrochloric, nitric and phosphoric acid solutions: effect of proton activity and anion participation. Hydrometall. 153, 179–189. https://doi.org/10.1016/J.HYDROMET.2015.02.002.

Bayramoglu, M., Demircilólu, N., Tekin, T., 1995. Dissolution kinetics of Mazidagi phosphate rock in HNO_3 solution. Int. J. Miner. Process. 43, 249–254. https://doi.org/10.1016/0301-7516(95)00010-B.

Becker Pierre, 1983. Phosphates And Phosphoric Acid Raw Materials, Technology and Economics of the Wet Proces. Compagnie Franqaise de VAzote and Duetag-France Paris. URL https://archive.org/details/beckerpierre.phosphatesandphosphoricacidrawmaterialstechnologyandeconomicsofthewetprocess.1983 (accessed 4.27.25).

Brahim, K., Soussi-Baatout, A., Khattech, I., Jemal, M., 2017. Dissolution kinetics of fluorapatite in the hydrochloric acid solution. J. Therm. Anal. Calorim. 129, 701–708. https://doi.org/10.1007/S10973-017-6221-8.

Calmanovici, C.E., Gilot, B., Laguerie, C., 1997. Mechanism and kinetics for the dissolution of Apatitic materials in acid solutions. Braz. J. Chem. Eng. 14, 95–102. https://doi.org/10.1590/S0104-66321997000200001.

Campbell, M.D., Martinez-Frias, J., Machairas, E., Varouchakis, E.A., 2023. Cost–Benefit Analysis and Risk Assessment for Mining Activities in Terms of Circular Economy and Their Environmental Impact. Geosciences 2023, Vol. 13, Page 318 13, 318. doi: 10.3390/GEOSCIENCES13100318.

Crundwell, F.K., 2013. The dissolution and leaching of minerals: mechanisms, myths and misunderstandings. Hydrometall. 139, 132–148. https://doi.org/10.1016/J.HYDROMET.2013.08.003.

Dorozhkin, S.V., 1997. Surface reactions of apatite dissolution. J. Colloid Interface Sci. 191, 489–497. https://doi.org/10.1006/JCIS.1997.4942.

Dreisinger, D., Abed, N., 2002. A fundamental study of the reductive leaching of chalcopyrite using metallic iron part I: kinetic analysis. Hydrometall. 66, 37–57. https://doi.org/10.1016/S0304-386X(02)00079-8.
Elmisaoui, S., Latifi, A.M., Khamar, L., 2024. Analysis of the dissolution of phosphate ore particles in phosphoric acid: influence of particle size distribution. Hydrometall. 223, 106197. https://doi.org/10.1016/J.HYDROMET.2023.106197.
Espiari, S., Rashchi, F., Sadrnezhaad, S.K., 2006. Hydrometallurgical treatment of tailings with high zinc content. Hydrometall. 82, 54–62. https://doi.org/10.1016/J.HYDROMET.2006.01.005.
Ethiopia, E.O., 1999. Kinetics of dissolution of phosphorite in acid mixtures. Bull. Chem. Soc. Ethiop. 13, 63–70. https://doi.org/10.4314/bcse.v13i1.21057.
European Commission, 2010. Antitrust: European Commission fines animal feed phosphates producers €175 647 000 for price-fixing and market-sharing in first "hybrid" cartel settlement case.
Faraji, F., Alizadeh, A., Rashchi, F., Mostoufi, N., 2022. Kinetics of leaching: a review. Rev. Chem. Eng. 38, 113–148. https://doi.org/10.1515/REVCE-2019-0073.
Ferket, P.R., van Heugten, E., van Kempen, T.A.T.G., Angel, R., 2002. Nutritional strategies to reduce environmental emissions from nonruminants. J. Anim. Sci. 80, E168–E182. https://doi.org/10.2527/ANIMALSCI2002.
Gbor, P.K., Jia, C.Q., 2004. Critical evaluation of coupling particle size distribution with the shrinking core model. Chem. Eng. Sci. 59, 1979–1987. https://doi.org/10.1016/J.CES.2004.01.047.
Gharabaghi, M., Irannajad, M., Noaparast, M., 2010. A review of the beneficiation of calcareous phosphate ores using organic acid leaching. Hydrometall. 103, 96–107. https://doi.org/10.1016/J.HYDROMET.2010.03.002.
Gilmour, R., 2013. Phosphoric acid: purification, uses, technology, and economics. Phosphoric Acid: Purificat. Uses Technol. Econ. 1–327. https://doi.org/10.1201/B16187.
Guan, Q., Sui, Y., Liu, C., Wang, Y., Zeng, C., Yu, W., Gao, Z., Zang, Z., Chi, R.A., 2022. Characterization and leaching kinetics of Rare Earth elements from phosphogypsum in hydrochloric acid. Minerals 12, 703. https://doi.org/10.3390/MIN12060703.
Habashi, F., 2017. From the SelectedWorks of Fathi Habashi Hydrochloric Acid in Hydrometallurgy.
Habbache, N., Alane, N., Djerad, S., Tifouti, L., 2009. Leaching of copper oxide with different acid solutions. Chem. Eng. J. 152, 503–508. https://doi.org/10.1016/J.CEJ.2009.05.020.
Hao, W., Björkman, E., Lilliestråle, M., Hedin, N., 2014. Activated carbons for water treatment prepared by phosphoric acid activation of hydrothermally treated beer waste. doi: 10.1021/IE5004569.S001.
Jin, Y., Ma, Y., Weng, Y., Jia, X., Li, J., 2014. Solvent extraction of Fe^{3+} from the hydrochloric acid route phosphoric acid by D2EHPA in kerosene. J. Ind. Eng. Chem. 20, 3446–3452. https://doi.org/10.1016/J.JIEC.2013.12.033.
Jung, M., Mishra, B., 2016. Kinetic and thermodynamic study of aluminum recovery from the aluminum smelter baghouse dust. J. Sustain. Metall. 2, 257–264. https://doi.org/10.1007/S40831-016-0056-6.
Khoshjavan, S., Rezai, B., 2011. Beneficiation of refractory rock phosphate by calcination and flotation. Miner. Metall. Process 28, 187–192. https://doi.org/10.1007/BF03402450.
Kim, C.J., Yoon, H.S., Chung, K.W., Lee, J.Y., Kim, S.D., Shin, S.M., Lee, S.J., Joe, A.R., Lee, S.I., Yoo, S.J., Kim, S.H., 2014. Leaching kinetics of lanthanum in sulfuric acid from rare earth element (REE) slag. Hydrometall. 146, 133–137. https://doi.org/10.1016/J.HYDROMET.2014.04.003.
Lassis, M., Mizane, A., Dadda, N., Rehamnia, R., 2015. Dissolution of Djebel Onk phosphate ore using sulfuric acid. Environ Nanotechnol Monit Manag 4, 12–16. https://doi.org/10.1016/J.ENMM.2015.03.002.
Liao, Y., Zhou, J., Huang, F., Wang, Y., 2015. Leaching kinetics of calcification roasting calcinate from multimetallic sulfide copper concentrate containing high content of lead and iron. Sep. Purif. Technol. 149, 190–196. https://doi.org/10.1016/J.SEPPUR.2015.05.042.
Liddell, K.C., 2005. Shrinking core models in hydrometallurgy: what students are not being told about the pseudo-steady approximation. Hydrometall. 79, 62–68. https://doi.org/10.1016/J.HYDROMET.2003.07.011.
Liu, K., Chen, Q., Yin, Z., Hu, H., Ding, Z., 2012. Kinetics of leaching of a Chinese laterite containing maghemite and magnetite in sulfuric acid solutions. Hydrometall. 125–126, 125–136. https://doi.org/10.1016/J.HYDROMET.2012.06.001.
Liu, W., Teng, L., Rohani, S., Qin, Z., Zhao, B., Xu, C.C., Ren, S., Liu, Q., Liang, B., 2021. CO_2 mineral carbonation using industrial solid wastes: a review of recent developments. Chem. Eng. J. 416, 129093. https://doi.org/10.1016/J.CEJ.2021.129093.
Liu, X., Wu, F., Qu, G., Jin, C., Liu, Y., Kuang, L., Li, H., Chen, X., Wang, Z., Cheng, Y., 2022. Application prospect of advanced oxidation technology in wet process phosphoric acid production. J. Environ. Chem. Eng. 10, 108868. https://doi.org/10.1016/J.JECE.2022.108868.
Lv, L., Zheng, D., Tang, S., Zhang, T., Liu, W., 2021. Phosphate ore particles dissolution kinetics in hydrochloric acid based on a structure-related segmented model. Powder Technol. 392, 141–149. https://doi.org/10.1016/J.POWTEC.2021.07.015.
Lv, X., Xiang, L., 2022. The generation process, impurity removal and high-value utilization of phosphogypsum material. Nanomaterials 2022 (12), 3021. https://doi.org/10.3390/NANO12173021.
Ma, H., Feng, X., Zeng, B., 2018. Self-anticorrosion for the combustion tower of heat recovered thermal process phosphoric acid production. Process Saf. Environ. Prot. 118, 330–347. https://doi.org/10.1016/J.PSEP.2018.07.008.
Madakkaruppan, V., Pius, A., Sreenivas, T., Giri, N., Sarbajna, C., 2016. Influence of microwaves on the leaching kinetics of uraninite from a low grade ore in dilute sulfuric acid. J. Hazard. Mater. 313, 9–17. https://doi.org/10.1016/J.JHAZMAT.2016.03.050.
Martin B. Hocking, 2005. Phosphorus and Phosphoric Acid. Academic Press.
Mendes, G.O., Murta, H.M., Valadares, R.V., Silveira, W.B., Silva, I.R., Costa, M.D., 2020. Oxalic acid is more efficient than sulfuric acid for rock phosphate solubilization. Miner Eng 155, 106458. https://doi.org/10.1016/J.MINENG.2020.106458.
Mgaidi, A., Mokni, H., 2018. Mathematical modeling of the dissolution of phosphate rock into various acidic medium. Hydrometall. 182, 27–31. https://doi.org/10.1016/J.HYDROMET.2018.09.013.
Olanipekun, E.O., 2003. Kinetics of acidulation reaction in nitrophosphate process. Int. J. Miner. Process. 69, 1–9. https://doi.org/10.1016/S0301-7516(01)00076-X.
Orabi, A., El-Sheikh, E., Hassanin, M., El Kady, M., Abdel-Khalek, M., Mowafy, A., 2018. Extraction of rare earth elements from Abu–Tartour wet process phosphoric acid using synthesized salicylaldehyde azine. Miner. Eng. 122, 113–121. https://doi.org/10.1016/J.MINENG.2018.03.037.
Poissonnier, J., Verberckmoes, A., Toch, K., Van Der Borght, K., Thybaut, J.W., 2021. Assessment of phosphate ore digestion kinetics and mixing behavior: a first step in unravelling NP-fertilizer production. Ind. Eng. Chem. Res. 60, 16599–16606. https://doi.org/10.1021/ACS.IECR.1C00936.
Rao, S., Yang, T., Zhang, D., Liu, W.F., Chen, L., Hao, Z., Xiao, Q., Wen, J.F., 2015. Leaching of low grade zinc oxide ores in NH_4Cl–NH_3 solutions with nitrilotriacetic acid as complexing agents. Hydrometall. 158, 101–106. https://doi.org/10.1016/J.HYDROMET.2015.10.013.
Rentería-Villalobos, M., Vioque, I., Mantero, J., Manjón, G., 2010. Radiological, chemical and morphological characterizations of phosphate rock and phosphogypsum from phosphoric acid factories in SW Spain. J. Hazard. Mater. 181, 193–203. https://doi.org/10.1016/J.JHAZMAT.2010.04.116.
Sevim, F., Saraç, H., Kocakerim, M.M., Yartaş, A., 2003. Dissolution kinetics of phosphate ore in H2SO4 solutions. Ind. Eng. Chem. Res. 42, 2052–2057. https://doi.org/10.1021/IE020168O.
Seyed Ghasemi, S.M., Azizi, A., 2018. Alkaline leaching of lead and zinc by sodium hydroxide: kinetics modeling. J. Mater. Res. Technol. 7, 118–125. https://doi.org/10.1016/J.JMRT.2017.03.005.
Sinirkaya, M., Özer, A.K., Gulaboglu, M.S., 2012. Kinetics of dissolution in H_2SO_4 of sulfated phosphate rock. Miner. Metall. Process 29, 156–158. https://doi.org/10.1007/BF03402253.
Sohn, H.Y., 1979. Fundamentals of the kinetics of heterogeneous reaction systems in extractive metallurgy. Rate Processes of Extractive Metallurgy 1–51. https://doi.org/10.1007/978-1-4684-9117-3_1.
Soltani, F., Abdollahy, M., Koleini, S.M.J., Moradkhani, D., 2017. Selection of an appropriate leaching method for light REEs from esfordi flotation concentrate based on mineral characterization. J. S. Afr. Inst. Min. Metall. 117, 443–450. https://doi.org/10.17159/2411-9717/2017/V117N5A6.
Soussi-Baatout, A., Brahim, K., Khattech, I., Kamoun, L., Jemal, M., 2018. Thermochemical and kinetic investigations of the phosphoric attack of Tunisian phosphate ore. J. Therm. Anal. Calorim. 131, 3121–3132. https://doi.org/10.1007/S10973-017-6825-Z/METRICS.
Soussi-Baatout, A., Ibrahim, K., Khattech, I., Jemal, M., 2016. Attack of Tunisian phosphate ore by phosphoric acid: kinetic study by means of differential reaction calorimetry. J. Therm. Anal. Calorim. 124, 1671–1678. https://doi.org/10.1007/S10973-016-5263-7/METRICS.
Sullivan, T.W., Douglas, J.H., Gonzalez, N.J., 1994. Levels of Various elements of concern in feed phosphates of domestic and foreign origin. Poult. Sci. 73, 520–528. https://doi.org/10.3382/PS.0730520.
Tayibi, H., Choura, M., López, F.A., Alguacil, F.J., López-Delgado, A., 2009. Environmental impact and management of phosphogypsum. J. Environ. Manage. 90, 2377–2386. https://doi.org/10.1016/J.JENVMAN.2009.03.007.
Wu, Z., She, L., Ye, P., Zhu, T., Li, J., Zhang, X., Ma, J., Wang, T., 2023. Extraction of H_3PO_4 from low-grade phosphate rocks leachate of HCl-route by the mixture of TBP and IPE: optimization, mass transfer and mechanism. J. Mol. Liq. 370, 120861. https://doi.org/10.1016/J.MOLLIQ.2022.120861.
Yartaşi, A., Kocakerim, M.M., Yapici, S., Özmetin, C., 1994. Dissolution kinetics of phosphate ore in SO_2-saturated water. Ind. Eng. Chem. Res. 33, 2220–2225. https://doi.org/10.1021/IE00033A028.
Yu, Y.H., Du, C.M., 2023. Leaching of phosphorus from phosphate tailings and extraction of calcium phosphates: toward comprehensive utilization of tailing resources. J. Environ. Manage. 347, 119159. https://doi.org/10.1016/J.JENVMAN.2023.119159.